Rheological Properties of Highly Concentrated Dense Packed Layer Emulsions (w/o) Stabilized by Asphaltene

Serkan Keleşoğlu [a,b], Albert Barrabino Ponce [a], Geir Humborstad Sørland [c], Sébastien Simon [a], Kristofer Paso [a], Johan Sjöblom [a]*

[a] Ugelstad Laboratory, Department of Chemical Engineering, Norwegian University of Science and Technology (NTNU), NO-7491 Trondheim, Norway

[b] Department of Process and Fluid Flow Technology, Institute for Energy Technology (IFE), NO-2007 Kjeller, Norway

[c] Anvendt Teknologi AS, NO-7022 Trondheim, Norway

Author Information

Corresponding Author and Author to Whom Correspondence Should be Addressed:

*Tel.: +47 465 42 746, E-mail: Serkan.Kelesoglu@ife.no

ABSTRACT

Dense packed layers (DPLs) were sedimented and removed from various asphaltene stabilized w/o emulsion batches, and contained aqueous phase volume fractions (ϕ) between 0.701 and 0.808. These values are close to the theoretical value of hexagonally close-packed spheres (0.74). Rheological properties of the DPLs were investigated using a rheometer equipped with plate-plate and cone-plate geometries. Flow curves and oscillatory shear measurements were obtained at 20^{o}C. Shear thinning and yield stress behaviour is observed. The measurements confirm the existence of a DPL yield stress which increases with the aqueous phase volume fraction. Hysteretic flow curve data show agreement with the Herschel-Bulkley relation. Oscillatory shear measurements within the linear viscoelastic regime are confirmed by strain-invariant values of G' (storage modulus) and G'' (loss modulus). Beyond the linear viscoelastic regime, non-linear relaxation processes are observed. The rheometric results indicate weak gel-like behaviour and a dispersed-fraction dependent gel strength. Correlated UV-Vis spectroscopy and NMR measurements indicate asphaltene adsorption amounts (Γ) of 1.95 mg.m^{-2} to 2.15 mg.m^{-2} and average surfaces areas per asphaltene molecule (σ) were in the range of 64 Å^2 to 69 Å^2 in the DPL.

KEYWORDS: Rheology; Dense Packed Layer; Asphaltene; Asphaltene Stabilized Emulsions; Water-in-Crude Oil Emulsions (w/o).

1. INTRODUCTION

Water-in-crude oil emulsions (w/o) are ubiquitous in the petroleum production industry. Emulsion formation commonly occurs during production, transport, and processing of crude oils. Emulsion formation in the presence of water requires agitation forces which may occur in pipes, pumps, and choke valves. The stability of w/o emulsions depends on chemical composition as well as energy input. Emulsion stability is enhanced by the presence of indigenous interfacially active substances such as, asphaltenes and resins. In addition, emulsions may be stabilized by dispersed inorganic particles present in crude oils. The increase in emulsion stability with time is related to the build-up and rearrangement of complex layers at the water-oil interface. [1–11]

In the petroleum industry, flow assurance and produced fluid quality are central concerns in promoting efficient separation processes of water from crude oils. The overall separation process may comprise several sub-processes, such as sedimentation, flocculation, coalescence, and creaming. Additional essential sub-processes may include dynamic surfactant release and diffusion, gravity enhanced interfacial coalescence, Brownian motion, convection processes, and etc.[12] Separation processes may be enhanced by means of chemical demulsification [13], thermal application [14], gravitational and centrifugal forces [15], and electrostatic coalescence [16-18].

Macro emulsions are thermodynamically unstable dispersions of oil and water. However, macro emulsions are often kinetically stabilized due to large activation energies associated with flocculation and/or coalescence processes. Coalescence comprises fusing of dispersed droplets and/or separated phases. Coalescence is driven by a free energy reduction associated with removal of interfacial energy. Destabilization of water-in-crude oil

emulsions under gravitational forces is illustrated in Fig. 1. Destabilization comprises three primary steps: (1) water droplet flocculation; (2) gravimetric sedimentation; and (3) coalescence. Subsequently, a free water layer is formed.[3, 19] In oil-water separators, emulsions can accumulate at the oil–water interface to form a thick viscous layer named dense-packed layer (DPL). This layer can reduce separation efficiency and upset the process.[20-25]

Formation of a stable and dense packed water-in-crude oil emulsion layer (DPL), as shown in Fig. 1, is a common occurrence during the gravitational separation processes. DPL is a thick and viscous layer primarily structured by emulsified water, and may also contain dispersed inorganic particles. Formation and growth of the DPL depends on sedimentation and as well as coalescence processes. The sedimentation rate depends not only on droplet size distribution, but also on density and viscosity phase differences. On the other hand, coalescence processes are mainly governed by interfacial properties of indigenous components. The formation of a DPL is intimately related to primary coalescence processes and associated release of indigenous stabilizers from the interface. These processes contribute to an enhanced stabilization of the remaining water droplets, and effectively inhibit subsequent coalescence processes. The surfactant release process is known as the "dynamic surfactant effect". Formation of DPL is undesirable and must be avoided in the petroleum industry to afford efficient separation processes. Indeed, DPLs are quite stable and reduce the separation rates. [12, 20-25]

Crude oils are complex mixtures containing millions of distinct molecular species. To simplify the study of crude oils in petroleum science, classification of indigenous components is based on SARA (refers to saturates, aromatics, resins, and asphaltenes,

respectively) fractionation is feasible. As such, indigenous crude components are separated on the basis of polarity, aromaticity, and solubility.[4, 26] Asphaltenes are the most polar and heaviest fraction of crude oils within the SARA classification. Resin-stabilized asphaltene aggregates exhibit interfacial activity. Moreover, resin-stabilized asphaltenes are primarily responsible for stabilizing water in crude oil emulsions. Several literature studies report emulsion stabilization properties of asphaltenes. [4, 27, 28] The studies successfully correlate chemical and physical properties of with the emulsion stability of the respective crude oil. Asphaltenes are soluble in toluene and chloroform but insoluble in non–polar aliphatic solvents. Asphaltenes may be precipitated using pentane, hexane, or heptane. Primary asphaltene molecules have a molecular weight in the range of 500 $g.mol^{-1}$ to 1000 $g.mol^{-1}$. Asphaltenes exhibit a tendency to self associate to form aggregates. The aggregate size depends on temperature, pressure, and nature of the solvent. [4, 27, 28]

Despite frequent formation of stable DPLs during separation processes, there is an absence of fundamental knowledge concerning DPL rheological characteristics. Knowledge of rheological properties of these systems may lead to improved predictions of DPL deformation and break up processes. Therefore, in the present investigation, a set of rheological properties is obtained for a model DPL. The DPLs were prepared by centrifugation from various batches of asphaltene stabilized model emulsions. Water contents were determined by Karl-Fischer titration. The rheological properties of the DPLs were investigated using a rheometer equipped with plate-plate and cone-plate geometries. Flow curves (shear stress vs. shear rate) and oscillatory deformation (strain and frequency sweep) measurements were performed at $20^{o}C$. In addition, droplet size distributions were determined using low field NMR [29-30]. Furthermore, adsorbed amounts of asphaltenes at the

interface were quantified by UV-Vis spectroscopy [31] and the stability of the DPL against coalescence was investigated under centrifugal forces.

2. EXPERIMENTAL SECTION

2.1. Materials

A North Sea heavy crude oil containing very small amounts of emulsified water (0.06 wt. %) and no additive chemicals was provided by Statoil ASA. Physico-chemical properties, SARA composition, water content, and density are presented in Table 1. The SARA fractions were determined according to Hannisdal et al.[32] Analytical grade sodium chloride (NaCl for analysis > 99.5 %) and xylene (AnalaR NORMAPUR®, mixture of 3 isomers + ethyl benzene: minimum 98.5 %) were received from Aldrich Chemical Company and VWR International. Synthetic brine containing 3.5% (w/v) in the Milli-Q water (resistivity of 18.3 MΩ.cm, Millipore, USA) was used as the aqueous phase. Model fluids were prepared with a constant 8 $g.L^{-1}$ asphaltene in xylene. Prior to emulsification, the asphaltene solution was first stirred overnight and subsequently sonicated for 30 minutes.

2.2. Methods

2.2.1. Extraction of Asphaltene from Crude Oil

Asphaltene extraction was performed as follows: the crude oil was initially heated to 60^{o}C for at least 4 hours and then shaken to provide homogenization. Subsequently, 4 g of crude oil was diluted to 160 mL with *n*-pentane and homogenized with a magnetic stirrer overnight to precipitate asphaltenes. The precipitated asphaltenes were first coarsely filtrated and then separated from the mixture using a 0.45 µm HVLP membrane filter (Millipore, USA). The extracted asphaltenes were dried under nitrogen. Elemental

composition of the extracted asphaltene is given in Table 2 and was determined by SGS Multilab (Evry, France) using thermal conductivity measurements for C, H, and N and infrared measurements for O and S.

2.2.2. Emulsion Formation and DPL Separation

To examine rheological properties, droplet size distribution, adsorption properties and coalescence properties, a model DPL system was prepared. A model fluid system was first selected, a model emulsion was formed, and a model DPL was separated from the emulsion using sequential gravimetric methods. Asphaltene in xylene was selected as the continuous model fluid phase. Synthetic brine was selected as the aqueous phase. Therefore, the extracted asphaltenes behave as the stabilizing agent in the multiphase model fluid system. The following procedure was used: 25 mL of synthetic brine and 25 mL of model oil (8 $g.L^{-1}$ asphaltene in xylene) were emulsified using an Ultra Turrax T 25 (18 mm head) from Ika® - Werke Co. (Germany) at 24,000 rpm for 3 minutes. Subsequently, the emulsion was gravimetrically separated for 16 hours at ambient temperature conditions ($23^{o}C \pm 1^{o}C$). After gravitational separation, the emulsion was centrifuged at 5,000 rpm for 15 minutes using an Eppendorf 5810. After centrifugation, a free water layer exists at the bottom of the centrifugation tube, a free oil layer exists at the top of the centrifugation tube, and a DPL is present between the free water and oil phases. The DPL was isolated and recovered by first removing the free oil and then water phases. The DPL was subjected to Karl-Fischer titration after gentle shaking for 1 minute to provide homogenization. Karl-Fischer measurements were performed using a KF Coulometer 831 (Metrohm AG, Switzerland) to quantify the water content of the separated DPL. The separated free oil phase was subjected to additional centrifugation at 5,000 rpm for 15 minutes and subsequently analyzed by UV-Vis

spectrocopy[29]. No additional analysis was performed on the free water phase. The DPL was retained for rheometric analysis.

The specific asphaltene concentration was selected in order to obtain an appreciable amount of DPL. Lower asphaltene concentration tended to yield sparse DPL quantities, and higher asphaltene concentrations hindered effective sedimentation processes. In addition, consideration was given to the energy input during emulsification, in order to provide a system in which sedimentation processes occur sufficiently fast to yield a DPL layer, but not overly rapid such as to cause complete separation of oil and water.

2.2.3. UV-Vis Spectroscopy

UV-Vis absorbance measurements were performed with a 2441 PC spectrophotometer (Shimadzu Corporation). The absorbance measurements were performed on only the free oil phase separated from the DPL formed emulsion. A 1 cm quartz measuring cell was used and the temperature was maintained at 20^{o}C. An absorbance wavelength of 336 nm was utilized. A calibration curve was first constructed by preparing a series of asphaltene solutions in xylene with concentrations ranging from 0.01 g.L^{-1} to 0.1 g.L^{-1}. A linear response was obtained with respect to asphaltene content in xylene. Prior to measurements of samples originating from the DPL system, the recovered free oil phase was diluted with xylene to comply with the calibration curve. The diluted oil phase was used in the UV-Vis absorbance measurements, providing a measure of the asphaltene content in the free oil phase.

2.2.4. Determination of DPL Droplet Size Distribution

Droplet size distribution of the DPL was measured at 28^{o}C (± 0.1^{o}C) using a 21 MHz low field NMR instrument (400 G/cm) supplied by Anvendt Teknologi AS (Norway) and Advanced Magnetic Resonance Ltd. (England). In the NMR measurements, the droplet size distribution was determined using a combination of Pulsed Field Gradient (PFG), Stimulated Echo (STE), and Carr-Purcell-Meimboom-Gill (CPMG) sequences for measuring H_2O diffusion within the DPL, resolving the water and oil phase signal and measuring attenuation processes.[33, 34] In this study, Anvendt Teknologi AS (Trondheim, Norway) provided the tool to perform a one dimensional inverse Laplace transform on the CPMG data to get the droplet size distribution of the DPLs.

2.2.5. Rheology of DPL

The separated DPL was shaken gently by hand for at least 1 minute prior to the rheology measurements. The rheological properties of the DPL were investigated using a Physica MCR 301 Rheometer (Anton Paar, Austria) at 20^{o}C (± 0.01^{o}C). Both plate-plate and cone-plate geometries were used. The top plate of the plate-plate and cone-plate geometries had a radius of 37.5 mm and 19.98 mm (with 2.01^{o} cone angle), respectively. With these geometries, the samples are submitted to a laminar shear flow. The shear rate is constant along the cone base diameter for the cone-plate geometry whereas it varies for the plate-plate geometry. Both used geometries were rough to eliminate the any wall slip effect during the rheology measurements.[35, 36] The temperature was maintained by Peltier elements. The gap heights for the plate-plate and cone-plate geometries were 0.5 mm and 0.057 mm, respectively. The following rheometric protocol was used: The DPL sample was first loaded onto the bottom plate of the geometry and the top plate was lowered to the

specified gap height. Xylene was placed into the solvent trap to reduce evaporation processes and the environmental chamber was lowered to cover the sample. Each DPL sample was pre-sheared at 50 s^{-1} for 3 minutes to afford an identical shear history to all samples.

Flow curve (shear stress vs. shear rate) measurements were performed on each DPL sample using the following protocol: the shear rate was increased (log ramp) from 0.1 s^{-1} to 100 s^{-1} and then decreased (log ramp) from 100 s^{-1} to 0.1 s^{-1} to obtain increasing and decreasing flow rate curves. Both increasing and decreasing flow curve data were recorded using 30 measurement points of 10 second duration.

Oscillatory shear rheology provides the viscoelastic response of the DPL. Deformation is applied in a sinusoidal form and the resulting mechanical response is measured. A strain sweep is performed to identify the linear viscoelastic regime (LVR), in which the deformation magnitudes are insufficient to degrade the material structure. [37, 38] The strain sweep was performed on each DPL at a frequency of 1 Hz. The oscillatory strain was ramped logarithmically from 0.01% and 100%. After the LVR is defined, a frequency sweep is performed within the LVR to reveal the nature of the investigated DPL.[37, 38]

2.2.6. Stability of DPL

The stability of the DPL against coalescence was investigated by performing *additional* centrifugation at various rotating speeds. The volumes of the separated oil phase, aqueous phase, and DPL were recorded for each specific speed.

The entire protocol was as follows: various batches of the asphaltene stabilized emulsions were prepared using an identical process as described in section 2.2.2.

Subsequently, all of the various batches were mixed together into a single DPL sample and homogenized by shaking gently. Water content of the combined sample was determined by Karl-Fischer. Subsequently, specific 10 mL samples were removed from the combined sample and placed into individual centrifugation tubes. Each specific 10 mL sample was subjected to centrifugation at a different rotational speed, within the range of 1,000 rpm to 11,000 rpm. The centrifugation duration was 10 minutes. After each centrifugation, the volumes of separated oil phase, aqueous phase and re-established DPL were recorded.

3. RESULTS AND DISCUSSION

Fig. 2a shows the photographic image of freshly prepared asphaltene stabilized emulsion. Fig. 2b shows a photographic image of the emulsion after 16 hours of gravitational separation. A small amount of free water and free oil is observed after 16 hours of gravitational separation, but no change in color is apparent in the emulsion phase. Fig. 2c shows a photographic image of the system after centrifugation. The 3 obtained layers are clearly evident. Fig. 2d shows the separated DPL after removal of the free phases. Fig. 2e shows a photographic image of the DPL after homogenization by shaking gently by hand. Conductivity measurements and drop tests confirmed that all separated DPLs were of w/o structure.

3.1. Droplet Size of DPL

When the covered mean free path of diffusing molecules ($\sqrt{6D_0t}$) is much larger than the cavity dimension (R_{cavity}) there is a case, in which the surface relaxation is absent in the solution of the diffusion propagator.[33] In this case, the closed droplet can be simplified to Eq. (1) from the attenuation of the NMR signal. [33, 34]

$$\left(\mathrm{I}/\mathrm{I}_0\right) \approx \mathrm{e}^{-(\gamma^2\delta^2 g^2 R^2)/5}, \tag{1}$$

where I_0 represents the initial NMR signal, γ is the gyromagnetic ratio, δ denotes the gradient pulse length, g represents the applied gradient strength and R is the radius of the droplet. It must be assumed that there is a droplet size distribution for heterogeneous systems and Eq. (1) is valid and can be used as long as $\sqrt{6D_0 t}$ is much higher than R_{cavity}. Eq. (1) can be also expressed as

$$\left(\mathrm{I}/\mathrm{I}_0\right) \approx \sum \xi_i \, \mathrm{e}^{-(\gamma^2\delta^2 g^2 R_i^2)/5}. \tag{2}$$

Where ξ_i denotes the volume fraction of the droplets by mean of the surface to volume ratio $(S/V)_i$. Eq. (2) can be expanded to Eq. (3) when the exponent in Eq. (2) is small for all i values and then the average value of the square of the droplet radius can be received by

$$\left(\mathrm{I}/\mathrm{I}_0\right) \approx \left(\sum \xi_i - \sum \xi_i \, \mathrm{e}^{-(\gamma^2\delta^2 g^2 R_i^2)/5}\right) = 1 - \left[(\gamma^2\delta^2 g^2 \overline{R^2})/5\right]. \tag{3}$$

In which, the average value of the square of the droplet radius is yielded by $\overline{R^2}$. An average value for the surface to volume ratio can be obtained from the measurements of the early departure from I_0 as a function of the applied gradient strength and then this can be utilized in combination with a transfer relaxation time distribution (T_2) and Eq. (4) to obtain a droplet size distribution.[29,30]

$$T_2 \approx (V/S\rho) \tag{4}$$

Eq. (4) couples the surface to volume ratio to the surface relaxivity (ρ). A procedure for finding a measure for ρ has been given by Opedal et. al [29], and using this approach we end up with droplet size distribution;

$$\frac{V}{S} \approx T_2 \overline{\left(\frac{1}{T_2}\right)} \times \overline{\left(\frac{S}{V}\right)^{-1}} \tag{5}$$

Where $\overline{\left(\frac{1}{T_2}\right)}$ and $\overline{\left(\frac{S}{V}\right)^{-1}}$ are the averages values found from analyzing the T_2 distribution and from the diffusion experiments.[29] Then we have solved out the surface relaxivity and we may denote the droplet size (or surface to volume ratio) by measurable quantities only.

Fig. 3 and Fig. 4 give the sequences for suppressing bulk water and/or oil phase, measuring the droplet size (average squared droplet radius) and the T_2 attenuation of the water droplets in an oil phase, respectively.[29, 30] In this case, the applied gradient pulse length (δ) was 800 μs and the τ value was 1.5 ms in the sequence (13 interval) and then the corresponding attenuations for the sequence in Fig. 3 can be expressed as

$$\left(\mathrm{I}/\mathrm{I}_0\right) \approx \mathrm{e}^{-\left[(\gamma^2\delta^2 g^2 D_{(t)})(\Delta+\frac{3\tau}{2}-\frac{\delta}{6})\right]} \mathrm{e}^{-\left(\frac{\Delta}{T_1}+\frac{4\tau}{T_2}\right)}. \tag{6}$$

Where $D_{(t)}$ is the molecular diffusion coefficient, Δ represents the z-storage delay, T_1 is the longitudinal relaxation time, T_2 gives the transverse relaxation time and 2τ is the inter echo spacing and then the corresponding attenuations for the sequence in Fig. 4 is written as

$$\left(\mathrm{I}/\mathrm{I}_0\right) \approx \mathrm{e}^{-\left[(\gamma^2\delta^2 g^2 D_{(t)})(\Delta+\frac{3\tau}{2}-\frac{\delta}{6})\right]} \mathrm{e}^{-\left(\frac{\Delta}{T_1}+\frac{4\tau}{T_2}\right)} \mathrm{e}^{-\left(\frac{2n\tau'}{T_2}\right)}. \tag{7}$$

Where, n denotes the echo number and τ' is the inter-echo spacing in the CPMG experiments which is used to measure the T_2.

Fig. 5 shows the volume based droplet size distributions determined using the low field NMR technique for DPLs formed with aqueous volume fractions varying from 0.729 to

0.761. Various aqueous fractions were observed, ranging from 0.729 to 0.761, despite the identical preparation procedure. Thus, a stochastic distribution in aqueous fraction is inherently attained from the DPL preparation procedure used in this investigation. The aqueous volume fractions indicate that the water content of each DPL is close to the theoretical value of hexagonally close-packed spheres (0.74). Furthermore, it has been shown by the low field NMR measurements that the droplet size distribution of the DPL are not significantly influenced by water content within the present range. Indeed, the droplet size of within the DPL varies between 1.5 μm to 20 μm, with an average droplet size of approximately 5 μm for the separated DPLs. No conclusive trend in DSD is evident with respect to aqueous fraction.

3.2. Flow Curves of DPL

Fig. 6a and Fig. 6b represent both the increasing and decreasing shear rate curves for the DPLs measured by the rheometer using the plate-plate and cone-plate geometries, respectively. The aqueous fractions of the DPL are in the range of 0.701 to 0.786. For the rheometric measurements, fresh DPLs were prepared with aqueous fractions in the range of 0.701 to 0.786. The general picture that emerges from the flow curves is the existence of a yield stress, and therefore a minimum shear stress must be applied to commence flow. It is observed that the yield stress increases with increasing aqueous fraction. The existence of the yield stress is also a strong indication of the interactions between the dispersed droplets. Furthermore, all DPLs exhibit shear thinning behaviour because the viscosity decreases when the shear rate increases (Fig. 6, Table 3 and Table 4). Hysteresis observed in Fig. 6a and Fig. 6b is ascribed to coalescence and water separation processes. The curves suggest that the initial dispersed state can not be recovered after the DPL structure is

altered by the flow curve experiments. Fig. 7 shows photographic images of the DPL before and after the flow curve experiments were imposed. Free water layers are clearly evident subsequent to the flow curves. These results confirm that the dispersed droplets coalesce and/or separate during shearing and the structure is altered.

In principle, the yield stress can be determined from flow curve measurements, oscillatory shear measurements, and creep measurements. [39-42] The yield stress of each DPL was estimated based on the flow curves as well as the oscillatory shear measurements.

By fitting the Herschel-Buckley relation to the flow curves, yield stress data can be estimated.[41] The Herschel-Bulkley equation (Eq. 8) was fitted to both increasing and decreasing shear rate portions of the measurements.

$$\tau = \tau_y + K\gamma^n, \tag{8}$$

where τ denotes the shear stress (Pa), τ_y is the yield stress (Pa), K gives the consistency index or viscosity (Pa.s), γ represents the shear rate (s^{-1}), and n is the flow behaviour index. The Herschel-Bulkley equation provides good fit to both portions of the flow curves. Regression coefficients (R^2) of at least 0.99 are obtained for all the DPLs cases except one. Table 3 and Table 4 give the obtained yield stress (τ_y), consistency index (K), and flow behaviour index (n) for all the DPLs estimated using the increasing and decreasing flow rate curves for both the plate-plate as well as the cone-plate geometries. The consistency index/viscosity and yield stress increase with increasing the water phase, indicating that the DPL is more viscous and more stress is required to initiate flow. Furthermore, the flow behaviour index (n) is less than unity for each DPL, confirming that the DPL exhibit shear thinning non-Newtonian flow behaviour.

3.3. Oscillatory Shear Rheology of DPL

3.3.1. Strain Sweep

Fig. 8a and Fig. 8b depict the variations of the storage modulus (G') and loss modulus (G'') for the DPL with water contents between 0.701 and 0.786 as a function of the shear stress at a constant frequency of 1 Hz measured by plate-plate and cone-plate geometries using the rheometer, respectively. It can be seen that not only the storage modulus but also the loss modulus are constant with increasing the shear stress up to a certain magnitude of the shear stress and then they both decrease with increasing shear stress using for both geometries, indicating that DPLs exhibit a transition from linear to non-linear viscoelastic behaviour as a function of the shear stress at a fixed frequency. The yield stress may be attributed to the specific shear stress value at which the measured storage modulus or loss modulus deviates from the linear viscoelastic regime response[37]. In the present study, the yield stress for each DPL was estimated based a criterion from the strain sweep of 5% tolerance from the linear viscoelastic regime for the both measuring geometries. Table 3 and Table 4 provide the yield stresses of the DPLs determined from the strain sweep measurements using the plate-plate and cone-plate geometries, respectively. It is clear from the obtained yield stress values that the required shear stress increases with increasing aqueous phase volume fractions. Moreover, a general picture emerges from comparison of the yield stress values is that the values determined from the flow measurements provide higher values than the oscillatory shear measurements for the plate-plate geometry. Cyclic degradation may account for the lower yield stress values from the oscillatory shear measurements. Laribi et al.[39] reported similar differences for smectite clay and observed that the obtained yield stress from the flow curve and creep recovery measurements are

numerically very close to each other, while the estimated yield stress values from the oscillatory shear measurements were found to be lower. Furthermore, Simon et al.[41] also reported similar results by yield stress values for particle stabilized emulsions. On the other hand, it is evident the comparison of Table 3 and Table 4 that the obtained yield stresses from the flow curves and oscillatory shear measurements are in relatively good agreement with the cone-plate geometry which exhibits uniform and defined deformation values. For the plate-plate geometry which exhibits inhomogeneous and ill-defined deformation, a larger divergence is obtained for the yield stress values.

Oscillatory shear measurements are also able to determine the flow point of a material. Flow point is defined as the intersection point of the storage modulus and loss modulus ($G' = G''$) and identifies the transition from gel character ($G' > G''$) to the liquid character ($G'' > G'$).[37, 38] As can be seen from Fig. 8 the storage modulus is higher than the loss modulus up to the flow point ($G' = G''$). Subsequently, the loss modulus is higher than the storage modulus for each DPL curve as a function of the shear stress. Hence the DPLs exhibit gel-like behaviour up to a critical deformation after which the gel-like behaviour changes to the liquid-like due to the deformation of the DPL as a function of the stress. Fig. 9 summarizes the determined flow points using the strain sweep measurements for each of the DPLs. It is observed that the flow point of the DPL increases non-linearly for higher water contents, indicating that more stress must be applied to induce flow. Furthermore, the data confirms a strong indication of a volume spanning network formation among the flocculated and interconnected droplets due to the high aqueous volume fractions, leading to a yield stress. Moreover, the type of geometry used to measure the flow point does not seem to influence the values obtained.

3.3.2. Frequency Sweep

Fig. 10a and Fig. 10b summarize the storage modulus (G') and loss modulus (G'') for each of the separated DPLs as a function of frequency at a constant oscillatory strain amplitude of 0.1% measured by plate-plate and cone-plate geometries, respectively. Applied strain during all the frequency sweep measurements was within the linear viscoelastic regime. The figure reveals a higher storage modulus than loss modulus at all frequency conditions. Both moduli are nearly constant with respect to frequency, confirming gel-like behavior for the DPLs of the asphaltene stabilized emulsions based on the definition of gels proposed by Almdal et al.[43]

From the frequency sweep measurements the strength of the gel-like character of a sample can be estimated using the magnitude of the storage modulus and the loss modulus ratio using the following criteria: [44]

- Samples having storage modulus (G') to loss modulus (G'') ratio lower than 1 show liquid-like behaviour.
- Samples having storage modulus (G') to loss modulus (G'') ratio between 1 and 10 are characterized as weak gel.
- Samples having storage modulus (G') to loss modulus (G'') ratio higher than 10 are characterized as strong gel.

The storage modulus and loss modulus at 1 Hz and the average of the moduli ratio over the whole investigated range of frequencies measured by plate-plate and cone-plate geometries for the DPLs are summarized in Fig. 11 and Fig. 12. It is evident from Fig. 11 that

a power law relationship exists between the storage modulus and also the loss modulus as a function of aqueous volume fraction. The slopes of the storage modulus and loss modulus have nearly identical magnitudes. Fig. 12 depicts the average ratio between the moduli frequencies between 0.1 Hz to 10 Hz for the DPL contained different water contents and measured by plate-plate and cone-plate geometries. The ratio changes between 4 and 6 indicating weak gel-like behaviour. Moreover, the storage modulus and loss modulus ratio increases almost linearly with increasing aqueous volume fraction.

Finally it must be highlighted that the rheological properties of DPL were analyzed using model systems (asphaltene dissolved in model solvent) and at laboratory conditions (atmospheric pressure and T=20°C). The conclusions obtained in these conditions need to be validated using real systems (real crude oil) in separation conditions present in gravity separators (higher pressures and temperatures). This is logical continuation of this study.

3.4. Adsorbed Amount of the Asphaltene in DPL

Fig. 13 shows the UV absorbance spectra of the asphaltene solution at various concentrations ranging from 0.01 $g.L^{-1}$ to 0.1 $g.L^{-1}$ in xylene and the constructed calibration curve at wavelength of 336 nm. It can be seen from the figure that absorbance increases as function of the concentration and the absorbance dependency is almost perfectly linear $(R^2 = 0.999)$ within the investigated concentration range.

Based on the UV depletion[31] measurements, the adsorbed amount of asphaltene (Γ) and surface area per molecule of the asphaltene (ϕ) are calculated using the following equations:

$$\Gamma = \frac{(C_i - C_f)V_{oil}}{S} \tag{9}$$

$$\sigma = \frac{M_w}{N\Gamma} \tag{10}$$

where C_i is the initial concentration of the asphaltene in the oil phase, C_f denotes the final concentration of the asphaltene in the oil phase after DPL separation, V_{oil} is the volume of the oil phase in the DPL, S is the total surface area of the droplets in the DPL, M_w denotes the molecular weight of the asphaltene and N is the Avogadro's number. The total surface area of the droplets in the DPLs was calculated based on droplet size measurements using low field NMR. The average molecular weight of the asphaltene molecule was assumed to be 750 g.mol^{-1}. [45-47]

Table 5 compares initial asphaltene concentrations in the oil phase, final asphaltene concentrations in the oil phase, adsorbed asphaltene amounts in the DPL (mg.m^{-2}) and surface areas per asphaltene molecule (σ) in the DPL as a function of aqueous phase volume fraction. The asphaltene concentration is reduced from 8 g.L^{-1} to around 6.4 g.L^{-1} for almost all DPLs, confirming that around 20% of the asphaltene was adsorbed in the DPLs. Furthermore, the absorbed amount of the asphaltene (Γ) and the surface area per molecule of the asphaltene (σ) in the DPLs varies between 1.95 mg.m^{-2} to 2.15 mg.m^{-2} and 64 Å^2 to 69 Å^2, respectively. Similar results were obtained at both liquid-liquid and solid-liquid interfaces in more diluted systems [31, 48, 49]. Therefore, the surface area per molecule of the asphaltene (σ) is similar in the DPL and in diluted systems (low aqueous phase volume fractions).

3.5. Stability of DPL against Coalescence

Fig. 14 displays amounts of separated aqueous phase, separated oil phase, and recovered DPL after centrifugation of the DPL at an aqueous volume fraction of 0.741. The

separated water and oil phases increase with increasing centrifugal force. Both the separated oil and aqueous phases increase but the applied centrifugal force was insufficient to drain all water from the DPL due to an uptake of water in the DPL subsequent to centrifugation. On the other hand, the volume of re-established DPL decreases nearly exponentially with increasing centrifugal force. Furthermore, it is observed that this DPL consists of approximately 81% water.

4. CONCLUSIONS

This study reports rheological properties of dense packed layer (DPL) from asphaltene stabilized emulsions (w/o) determined using a modern rheometer equipped with plate-plate and cone-plate measuring geometries. Flow curves and oscillatory shear measurements are performed at 20^{o}C. The results show that DPLs exhibit shear thinning and yield stress behaviours, following the Herschel-Bulkley relation. The aqueous volume fraction of the DPLs is close to the theoretical value of the hexagonally close-packed of spheres (0.740). Both the flow curve and strain sweep measurements confirm the existence of a yield stress. The value of the yield stress increases with increasing aqueous volume fraction. The Herschel-Bulkley equation fits well to both increasing and decreasing shear rate curves for the model systems tested and under the conditions applied (i.e. T=20°C and atmospheric pressure). Frequency sweep measurements within the linear viscoelastic regime indicate that the storage modulus ($G^{'}$) is higher than the loss modulus ($G^{''}$) and $G^{'}/G^{''}$ ratio changes between 4 and 6 over the investigated frequency range, indicating that the DPLs show weak gel-like behaviour. UV-Vis and NMR measurements indicate that asphaltene concentration (Γ) varies from 1.95 mg.m^{-2} to 2.15 mg.m^{-2} in the DPL. Average surfaces areas per asphaltene molecule (σ) are between 64 Å^2 and 69 Å^2. These values are similar to the one

obtained at both liquid-liquid and solid-liquid interfaces in more diluted systems. Consequently, the surface area per asphaltene molecule is therefore similar in diluted systems (low water cuts) and in the DPL. The influence of the asphaltenes present at the droplet interface on the rheology and stability of DPL has not been determined in this article. This could be assessed by varying the composition of the droplet interface and measuring the resultant DPL properties.

Acknowledgements

The authors gratefully acknowledge financial support for this work from the Research Council of Norway (NFR) and the industrial consortium JIP-1 (Joint Industrial Project) consisting of AkzoNobel, BP, Champion Technologies, Hamworthy, Saudi Aramco, Shell, Statoil ASA, and Total.

References

(1) Fingas, M.; Fieldhouse, B.; Bobra, M.; Tennyson, E., The Physics and Chemistry of Emulsions. In *Proceedings of the Workshop on Emulsions*, Marine Spill Response Corporation, Washington, D.C, 1993.

(2) Aske, N.; Kallevik, H.; Sjöblom, J., Water-in-crude oil emulsion stability studied by critical electric field measurements. Correlation to physico-chemical parameters and near-infrared spectroscopy. *J. Pet. Sci. Eng.* **2002,** *36* (1-2), 1-17.

(3) Schramm, L. L., *Emulsions: fundamentals and applications in the petroleum industry*. American Chemical Society: 1992.

(4) Sjöblom, J.; Aske, N.; Auflem, H. I.; Brandal, Ø.; Havre, T. E.; Sæther, Ø.; Westvik, A.; Johnsen, E. E.; Kallevik, H., Our current understanding of water-in-crude oil emulsions.: Recent characterization techniques and high pressure performance. *Adv. Colloid Interface Sci.* **2003,** *100-102*, 399-473.

(5) McLean, J. D.; Kilpatrick, P. K., Effects of asphaltene aggregation in model heptane-toluene mixtures on stability of water-in-oil emulsions. *J. Colloid Interface Sci.* **1997,** *196* (1), 23-34.

(6) McLean, J. D.; Kilpatrick, P. K., Effects of asphaltene solvency on stability of water-in-crude-oil emulsions. *J. Colloid Interface Sci.* **1997,** *189* (2), 242-253.

(7) Wu, X., Investigating the stability mechanism of water-in-diluted bitumen emulsions through isolation and characterization of the stabilizing materials at the interface. *Energy Fuels* **2002,** *17* (1), 179-190.

(8) Czarnecki, J.; Moran, K., On the stabilization mechanism of water-in-oil emulsions in petroleum systems. *Energy Fuels* **2005,** *19* (5), 2074-2079.

(9) Sullivan, A. P.; Kilpatrick, P. K., The effects of inorganic solid particles on water and crude oil emulsion stability. *Ind. Eng. Chem. Res.* **2002,** *41* (14), 3389-3404.

(10) Yan, N.; Gray, M. R.; Masliyah, J. H., On water-in-oil emulsions stabilized by fine solids. *Colloids Surf., A* **2001,** *193* (1-3), 97-107.

(11) Auflem, I. H.; Kallevik, H.; Westvik, A.; Sjöblom, J., Influence of pressure and solvency on the separation of water-in-crude-oil emulsions from the North Sea. *J. Petrol Sci. Eng.* **2001,** 31 (1), 1-12.

(12) Grimes, B.E; Dorao, C.A.; Simon, S.; Nordgård, E.L.; Sjöblom, J., Analysis dynamic surfactant mass transfer and its relationship to the transient stabilization of coalescing liquid-liquid dispersions. *J. Colloid Interface Sci.* **2010,** *348* (2), 479-490.

(13) Wu, J.; Xu, Y.; Dabros, T.; Hamza, H., Effect of demulsifier properties on destabilization of water-in-oil Emulsion. *Energy Fuels* **2003,** *17* (6), 1554-1559.

(14) Lissant, K. J., *Demulsification: industrial applications*. M. Dekker: New York, 1983.

(15) Dezhi, S.; Chung, J. S.; Xiaodong, D.; Ding, Z., Demulsification of water-in-oil emulsion by wetting coalescence materials in stirred-and packed-columns. *Colloids Surf., A* **1999,** *150* (1-3), 69-75.

(16) Mori, Y.; Tanigaki, M.; Maehara, N.; Eguchi, W., Effect of frequency in a.c. high voltage on coalescence of water-in-oil emulsion stabilized with sorbitan monooleate type nonionic surfactant. *J. Chem. Eng. Jpn.* **1994,** *27* (3), 340-343.

(17) Less, S.; Hannisdal, A.; Bjørklund, E.; Sjöblom, J., Electrostatic destabilization of water-in-crude oil emulsions: Application to a real case and evaluation of the Aibel VIEC technology. *Fuel* **2008,** *87* (12), 2572-2581.

(18) Less, S.; Vilagines, R. The electrocoalescers' technology: advances, strengths and limitations for crude oil separation. *J. Petrol. Sci. Eng.* **2012**, 81, 57-63.

(19) Holmberg, K.; Jönsson, B.; Kronberg, B.; Lindman, B., *Surfactants and Polymers in Aqueous Solution*. 2 ed.; Wiley: 2002.

(20) Czarnecki, J.; Moran, K.; Yang, X., On the "rag layer" and diluted bitumen froth dewatering. *Can. J. Chem. Eng.* **2007,** *85* (5), 748-755.

(21) Hartland, S., The effect of gravity on the drainage of thin films in two-dimensional dense-packed dispersions. *Chem. Eng. Sci.* **1979,** *34* (4), 485-491.

(22) Hartland, S.; Vohra, D. K., Effect of interdrop forces on the coalescence of drops in close-packed dispersions. *J. Colloid Interface Sci.* **1980,** *77* (2), 295-316.

(23) Hartland, S.; Jeelani, S. A. K., Choice of model for predicting the dispersion height in liquid/liquid gravity settlers from batch settling data. *Chem. Eng. Sci.* **1987,** *42* (8), 1927-1938.

(24) Hartland, S.; Jeelani, S. A. K., Prediction of sedimentation and coalescence profiles in a decaying batch dispersion. *Chem. Eng. Sci.* **1988,** *43* (9), 2421-2429.

(25) Khatri, N. L.; Andrade, J.; Baydak, E. N.; Yarranton, H. W., Emulsion layer growth in continuous oil-water separation. *Colloids Surf., A* **2011,** *384* (1-3), 630-642.

(26) Meléndez, L. V.; Lache, A.; Orrego-Ruiz, J. A.; Pachón, Z.; Mejía-Ospino, E. Prediction of the SARA analysis of Colombian crude oils using ATR–FTIR spectroscopy and chemometric methods. *J. Petrol. Sci. Eng.* 2012, 90–91, 56-60.

(27) Kilpatrick, P. K.; Spiecker, P. M., Asphaltene Emulsions. In *Encyclopedic Handbook of Emulsion Technology*, CRC Press: 2001; pp 707-730.

(28) Angle, C. W., Chemical Demulsification of Stable Crude Oil and Bitumen Emulsions in Petroleum Recovery-A Review. In *Encyclopedic Handbook of Emulsion Technology*, CRC Press: 2001; pp 541-594.

(29) Opedal, N. T.; Sørland, G. H.; Sjöblom, J., Methods for droplet size distribution determination of water-in-oil emulsions using low-field NMR. *Diffusion Fundamentals* **2009,** *7*, 1-29.

(30) Sørland, G. H.; Keleşoğlu, S.; Simon, S.; Sjöblom, J., Rapid characterization of emulsions by pulsed field gradient nuclear magnetic resonance. *Diffusion Fundamentals* **2013,** *18*, 1-16.

(31) Dudášova, D.; Simon, S.; Hemmingsen, P.L.; Sjöblom, J., Study of asphaltene adsorption onto different mineral and clays: Part 1. Experimental adsorption with UV depletion detection. *Colloids Surf., A* **2008,** *314* (1-3), 1-9.

(32) Hannisdal, A.; Hemmingsen, P. V.; Sjöblom, J., Group-type analysis of heavy crude oils using vibrational spectroscopy in combination with multivariate analysis. *Ind. Eng. Chem. Res.* **2005,** *44* (5), 1349-1357.

(33) Packer, K. J.; Rees, C., Pulsed NMR studies of restricted diffusion. I. Droplet size distributions in emulsions. *J. Colloid Interface Sci.* **1972,** *40* (2), 206-218.

(34) Balinov, B.; Söderman, O., Emulsion-the NMR Perspective. In *Encyclopedic Handbook of Emulsion Technology*, CRC Press: 2001; pp 279-303.

(35) Barnes, H. A., A review of the slip (wall depletion) of polymer solutions, emulsions and particle suspensions in viscometers: its cause, character, and cure. *J. Non-Newtonian Fluid Mech.* **1995,** *56* (3), 221-251.

(36) Bertola, V.; Bertrand, F.; Tabuteau, H.; Bonn, D.; Coussot, P., Wall slip and yielding in pasty materials. *J. Rheol.* **2003,** *47* (5), 1211-1226.

(37) Mezger, T. G., *The Rheology Handbook: For Users of Rotational and Oscillatory Rheometers*. Vincentz Network: 2006.

(38) Norton, I. T.; Spyropoulos, F.; Cox, P., *Practical Food Rheology: An Interpretive Approach*. Blackwell Publishing Ltd.: 2011.

(39) Laribi, S.; Fleureau, J.-M.; Grossiord, J.-L.; Kbir-Ariguib, N., Comparative yield stress determination for pure and interstratified smectite clays. *Rheol. Acta* **2005,** *44* (3), 262-269.

(40) Struble, L. J.; Schultz, M. A., Using creep and recovery to study flow behavior of fresh cement paste. *Cem. Concr. Res.* **1993,** *23* (6), 1369-1379.

(41) Simon, S.; Theiler, S.; Knudsen, A.; Øye, G.; Sjöblom, J., Rheological properties of particle-stabilized emulsions. *J. Dispersion Sci. Technol.* ***2010,*** *31* (5), 632-640.

(42) Al-Zahrani, S. M. A generalized rheological model for shear thinning fluids. *J. Petrol. Sci. Eng.* **1993**, 17 (3–4), 211-215.

(43) Almdal, K.; Dyre, J.; Hvidt, S.; Kramer, O., Towards a phenomenological definition of the term 'gel'. *Polym. Gels Netw.* **1993,** *1* (1), 5-17.

(44) Clark, A.; Ross-Murphy, S., Structural and mechanical properties of biopolymer gels. In *Biopolymers*, Springer Berlin Heidelberg: 1987; Vol. 83, pp 57-192.

(45) Groenzin, H.; Mullins, O.C.; Eser, S.; Mathews, J.; Yang, M.G.; Jones, D., Molecular size of asphaltene solubility fractions. *Energy Fuels* **2003,** 17, 498-503.

(46) Groenzin, H.; Mullins, O.C., Asphaltene molecular size. *J. Phys. Chem. A* **1999,** 103 (50), 11237-11245.

(47) Hortal, A.R.; Martinez-Haya, B.; Lobato, M.D.; Pedrosa J.M.; Lago, S., On the determination of molecular weight distributions of asphaltenes and their aggregates in laser desorption ionization experiments. *J. Mass Spectrom.* **2006,** 41(7), 960-968.

(48) Jestin, J.; Simon, S.; Zuponcic, L.; Barré, L., A small angle neutron scattering study of the adsorbed asphaltene layer in water-hydrocarbon emulsions: structural description related stability. *Langmuir* **2007,** 23(21), 10471-10478.

(49) Simon, S.; Jestin, J.; Palermo, T.; Barré, L., Relation between solution and interfacial properties of asphaltene aggregates. *Energy Fuels* **2009,** 23(1), 306-313.

Figure Captions:

Fig. 1. Destabilization of crude oil emulsions (w/o) under gravitational force.

Fig. 2. Photographic images of freshly prepared asphaltene stabilized emulsion (a) after 16 hours under gravitational separation (b) after centrifugation (c) separated dense packed layer (d) and homogenized dense packed layer (e) (The volume fraction of the aqueous phase in the DPL is 0.749 in this case).

Fig. 3. The combined spoiler recovery-13 interval Pulsed Field Gradient Stimulated Echo (PFGSTE) sequence with convection compensation.

Fig. 4. The combined spoiler recovery-13 interval Pulsed Field Gradient Stimulated Echo (PFGSTE) - Carr-Purcell-Meiboom-Gill (CPMG) sequence.

Fig. 5. Volume based droplet size distributions of the DPL contained different aqueous volume fractions (ϕ).

Fig. 6. Increasing and decreasing shear rate vs. shear stress curves measured by plate-plate (a) and cone-plate (b) geometries for the DPL contained different aqueous volume fractions (ϕ) (T= 20^{o}C).

Fig. 7. Photographic images of the DPL before (a) and after (b) the flow experiments (shear rate vs. shear stress curves) (The aqueous phase volume fraction in the DPL was 0.786 in this case and the used geometry was cone-plate, T=20^{o}C).

Fig. 8. Storage modulus ($G^{'}$) and loss modulus ($G^{''}$) as a function of stress at 1Hz measured by plate-plate (a) and cone-plate (b) geometries for the DPL contained different aqueous volume fractions (ϕ) (Filled symbols: Storage modulus, Open symbols: Loss modulus, T=20^{o}C).

Figure Captions (Continued):

Fig. 9. Flow point ($G' = G''$) at 1 Hz measured by plate-plate and cone-plate geometries for the DPL contained different aqueous volume fractions (ϕ) (T=20^{o}C).

Fig. 10. Storage modulus (G') and loss modulus (G'') measured by plate-plate (a) and cone-plate (b) geometries for the DPL contained different aqueous volume fractions (ϕ) (Filled symbols: Storage modulus, Open symbols: Loss modulus, Strain=0.1 %, T=20^{o}C).

Fig. 11. Storage modulus (G') and loss modulus (G'') at 1 Hz measured by plate-plate and cone-plate geometries for the DPL contained different aqueous volume fractions (ϕ) (Strain=0.1 %, T=20^{o}C).

Fig. 12. Average storage modulus (G') and loss modulus (G'') ratio over the investigated frequency range from 0.1 Hz to 10 Hz measured by plate-plate and cone-plate geometries for the DPLs contained different aqueous volume fractions (ϕ) (Strain=0.1 %, T=20^{o}C).

Fig. 13. UV-Vis absorbance spectra of the asphaltene solutions at different concentrations in xylene and the constructed calibration curve at 336 nm (T=20^{o}C).

Fig. 14. Separated water and oil percentages from the DPL as a function of rotational speed of centrifuge and water content of the re-established DPL after each centrifugation (Asphaltene concentration in xylene = 8 g/L, Volume of DPL = 10 mL, Aqueous phase volume fraction in the DPL=0.745, T=20^{o}C).

Table Headings:

Table 1. Physico-chemical properties of the crude oil used to extract the asphaltene in this study.

Table 2. Elemental composition of the asphaltene used in this study.

Table 3. The yield stress (τ_y), consistency index (K), and flow behaviour index (n) of the DPLs separated from various batch of the asphaltene stabilized emulsions and contained different aqueous phase volume fractions (ϕ) determined from flow curve and oscillatory shear measurements using "plate-plate geometry" (T= 20^{o}C).

Table 4. The yield stress (τ_y), consistency index (K), and flow behaviour index (n) of the DPLs separated from various batch of the asphaltene stabilized emulsions and contained different aqueous phase volume fractions (ϕ) determined from flow curve and oscillatory shear measurements using "cone-plate geometry" (T= 20^{o}C).

Table 5. Initial concentration of the asphaltene in oil phase, final concentration of the asphaltene in oil phase after separation of the DPL from the emulsion, aqueous phase volume fraction of the separated DPL, adsorbed amount of the asphaltene in the DPL (mg.m^{-2}) and surface area per molecule of the asphaltene (σ) in the DPL determined for various batches of the asphaltene stabilized emulsions (w/o) (T=20^{o}C).

Figures:

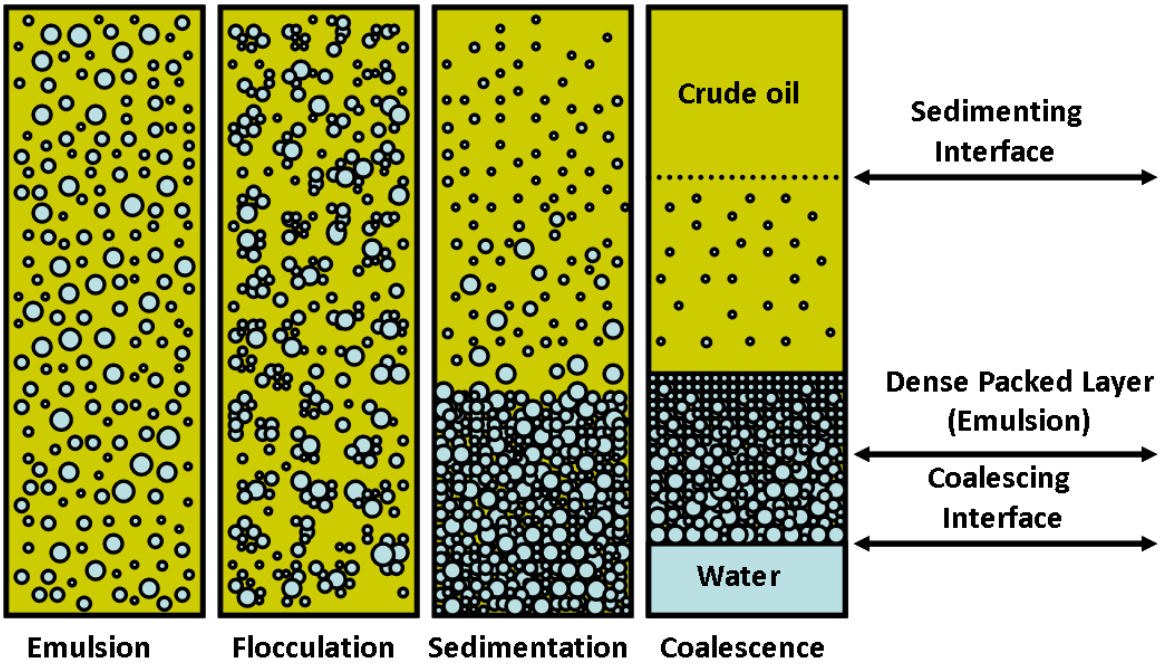

Fig. 1. Destabilization of crude oil emulsions (w/o) under gravitational force.

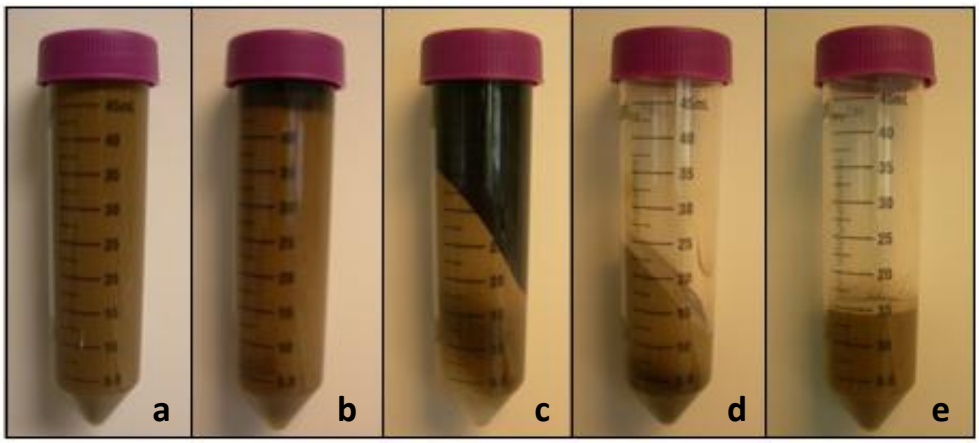

Fig. 2. Photographic images of freshly prepared asphaltene stabilized emulsion (a) after 16 hours under gravitational separation (b) after centrifugation (c) separated dense packed layer (d) and homogenized dense packed layer (e) (The volume fraction of the aqueous phase in the DPL is 0.749 in this case).

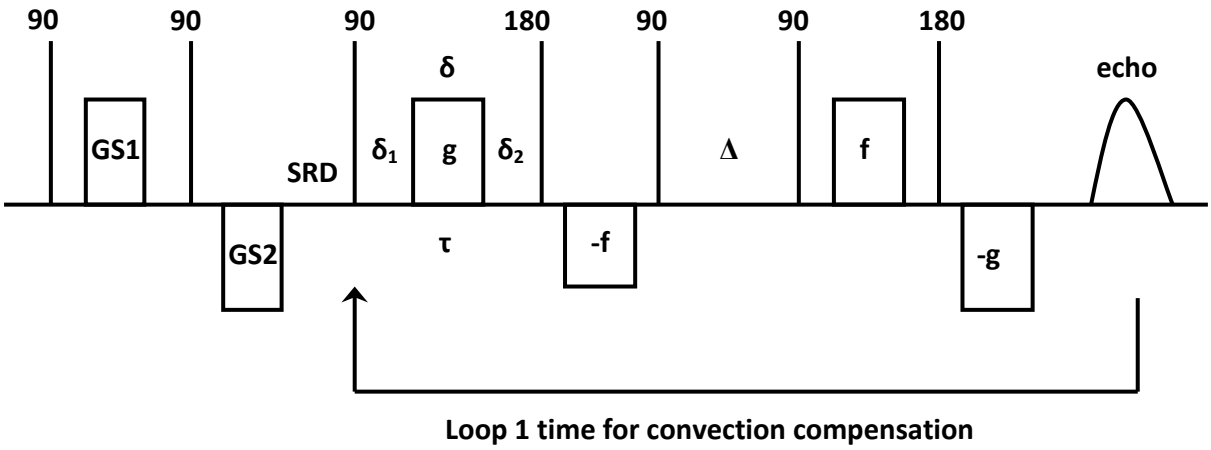

Fig. 3. The combined spoiler recovery-13 interval Pulsed Field Gradient Stimulated Echo (PFGSTE) sequence with convection compensation.

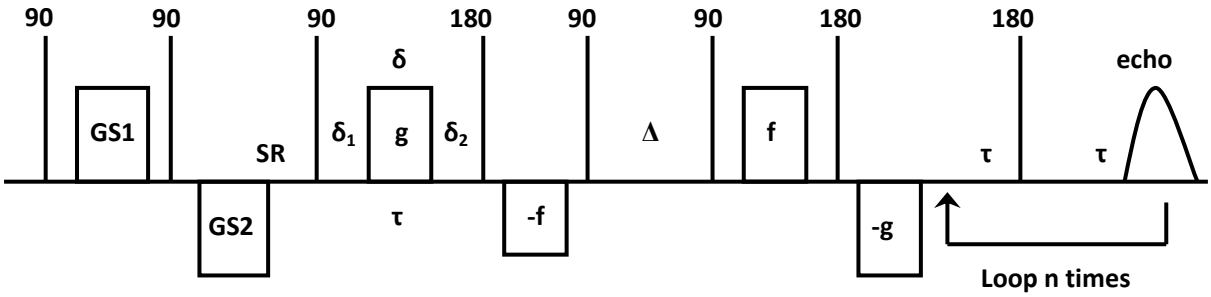

Fig. 4. The combined spoiler recovery-13 interval Pulsed Field Gradient Stimulated Echo (PFGSTE) - Carr-Purcell-Meiboom-Gill (CPMG) sequence.

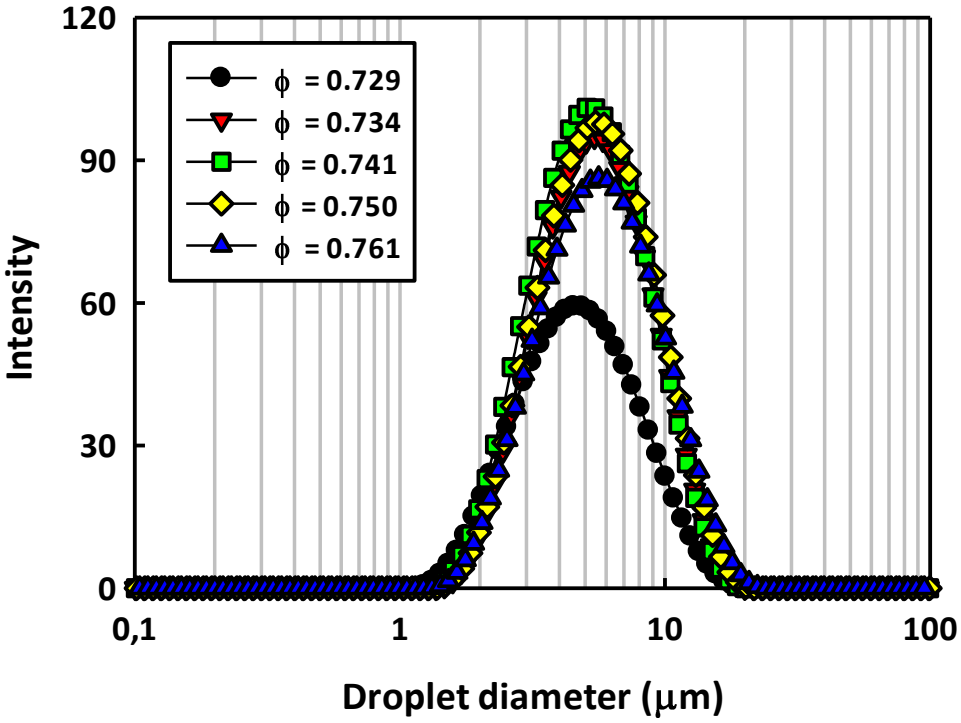

Fig. 5. Volume based droplet size distributions of the DPL contained different aqueous volume fractions (ϕ).

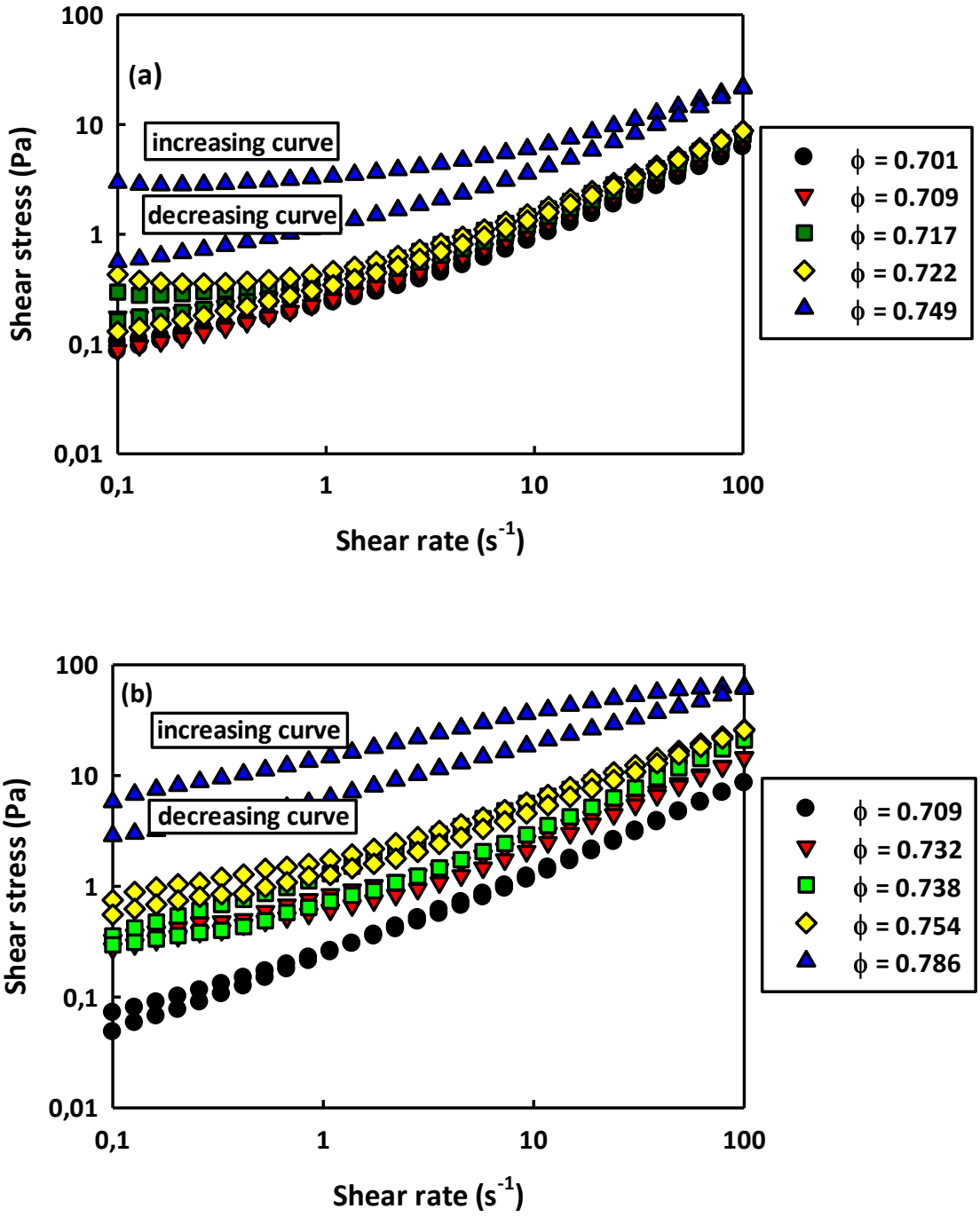

Fig. 6. Increasing and decreasing shear rate vs. shear stress curves measured by plate-plate (a) and cone-plate (b) geometries for the DPL contained different aqueous volume fractions (ϕ) (T= 20^{o}C).

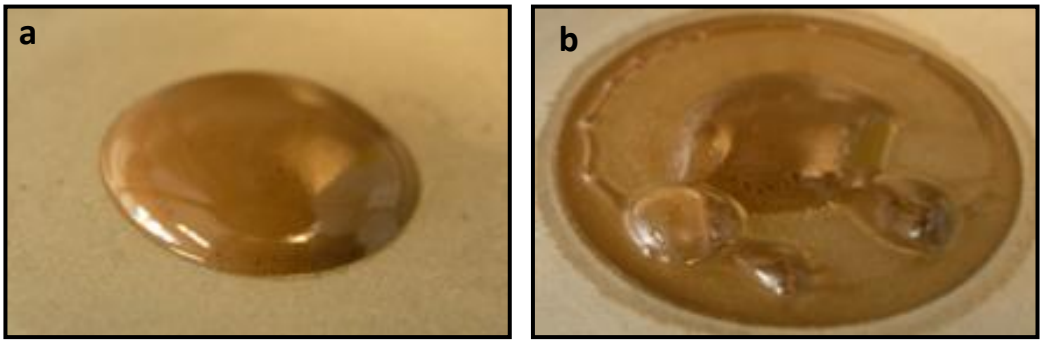

Fig. 7. Photographic images of the DPL before (a) and after (b) the flow experiments (shear rate vs. shear stress curves) (The aqueous phase volume fraction in the DPL was 0.786 in this case and the used geometry was cone-plate, T=20^{o}C).

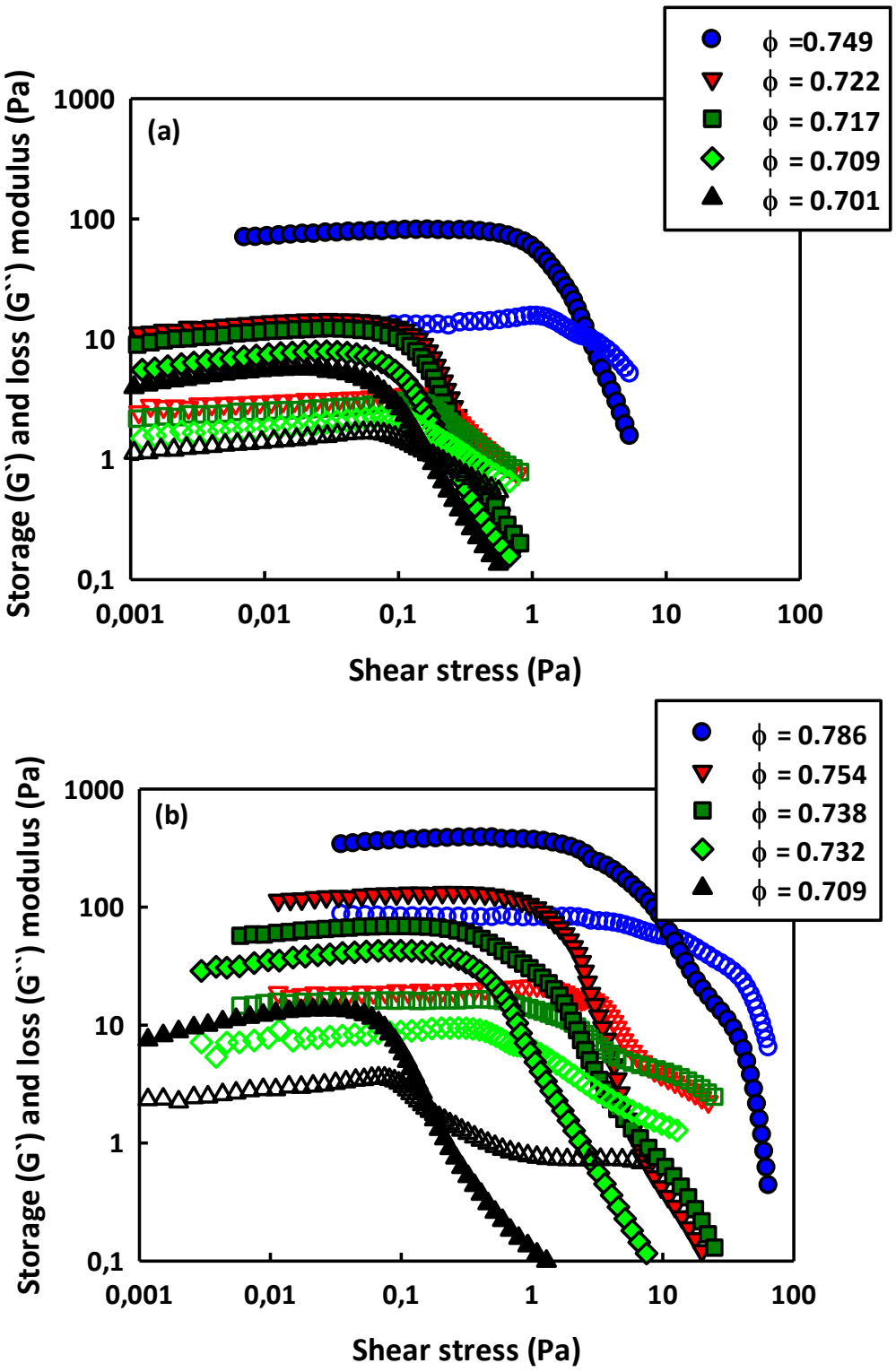

Fig. 8. Storage modulus ($G^{'}$) and loss modulus ($G^{''}$) as a function of stress at 1Hz measured by plate-plate (a) and cone-plate (b) geometries for the DPL contained different aqueous volume fractions (ϕ) (Filled symbols: Storage modulus, Open symbols: Loss modulus, T=20^{o}C).

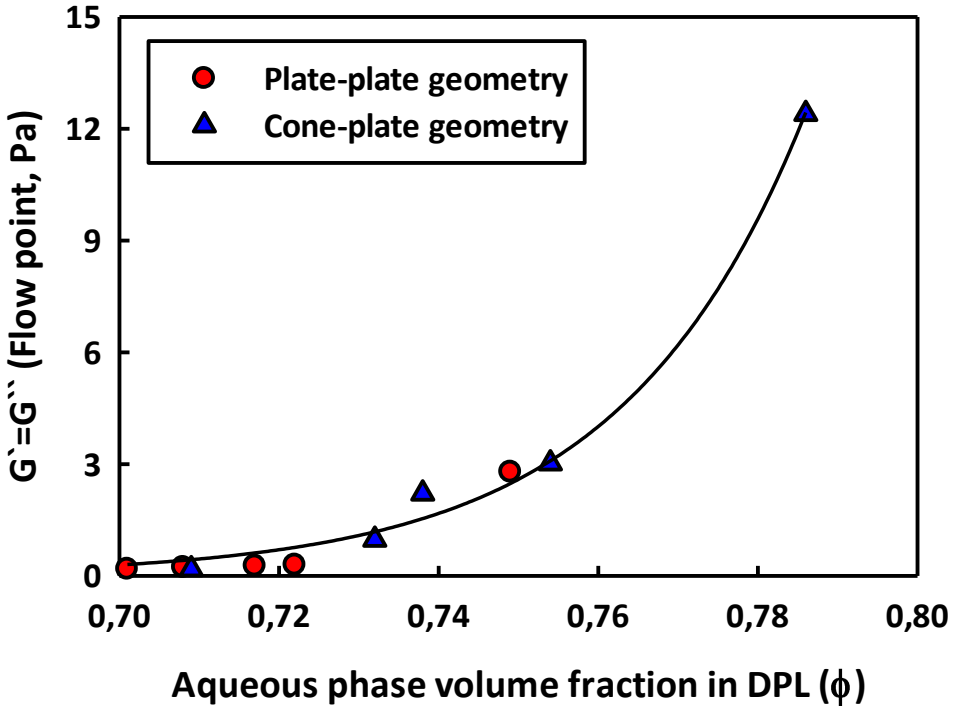

Fig. 9. Flow point ($G' = G''$) at 1 Hz measured by plate-plate and cone-plate geometries for the DPL contained different aqueous volume fractions (ϕ) (T=20^{o}C).

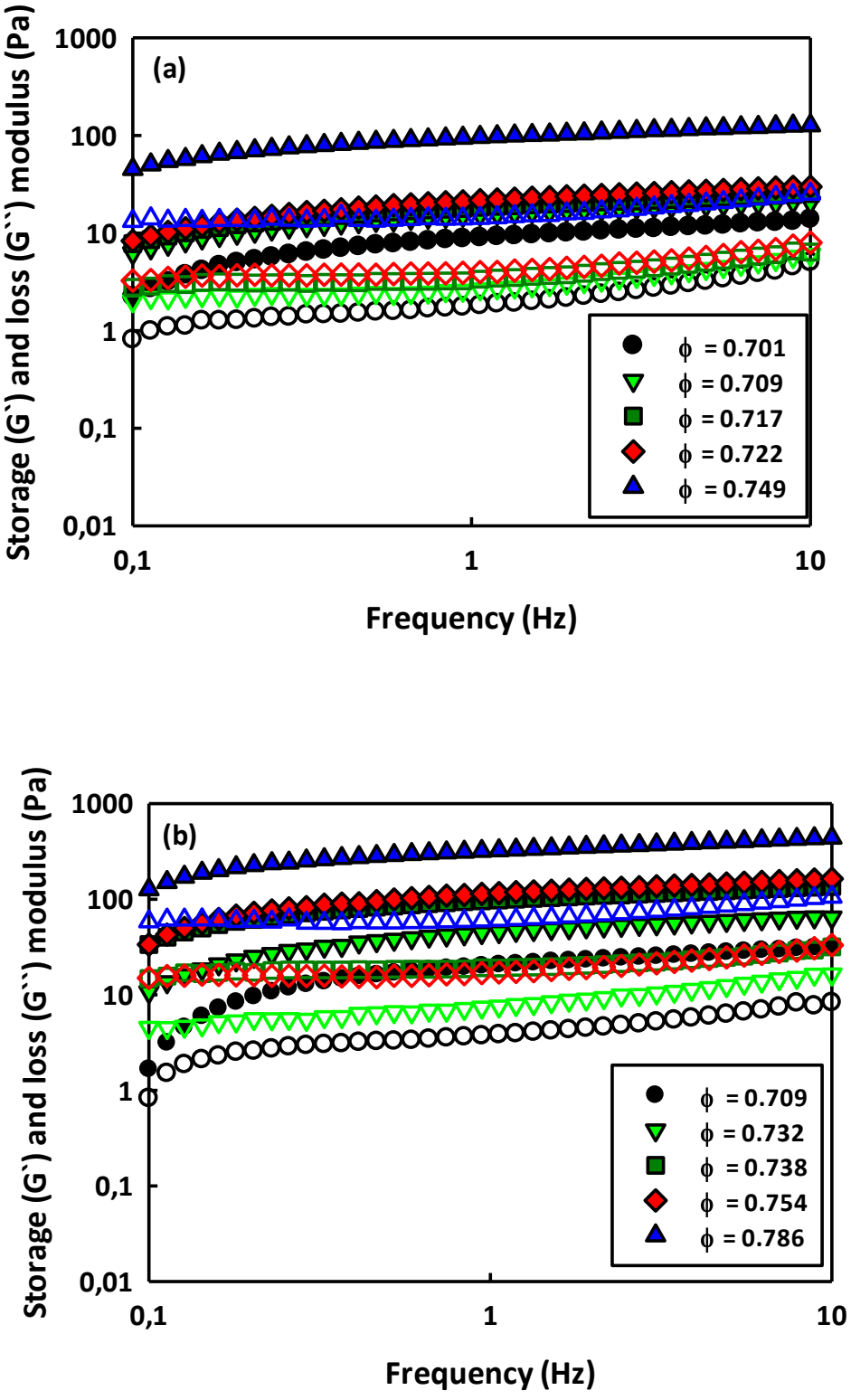

Fig. 10. Storage modulus ($G^{'}$) and loss modulus ($G^{''}$) measured by plate-plate (a) and cone-plate (b) geometries for the DPL contained different aqueous volume fractions (ϕ) (Filled symbols: Storage modulus, Open symbols: Loss modulus, Strain=0.1 %, T=20^{o}C).

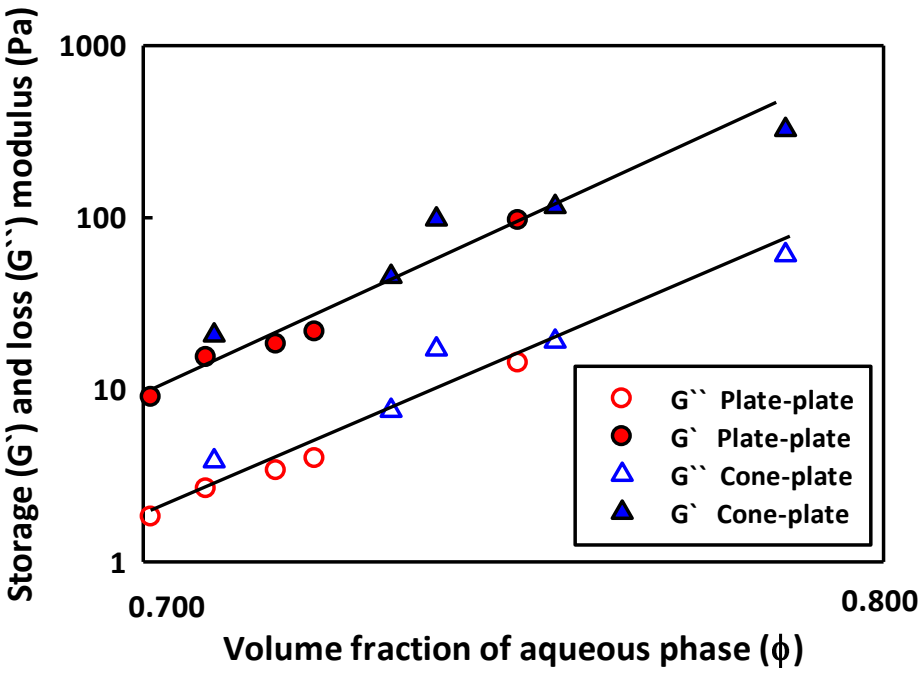

Fig. 11. Storage modulus ($G^{'}$) and loss modulus ($G^{''}$) at 1 Hz measured by plate-plate and cone-plate geometries for the DPL contained different aqueous volume fractions (ϕ) (Strain=0.1 %, T=20^{o}C).

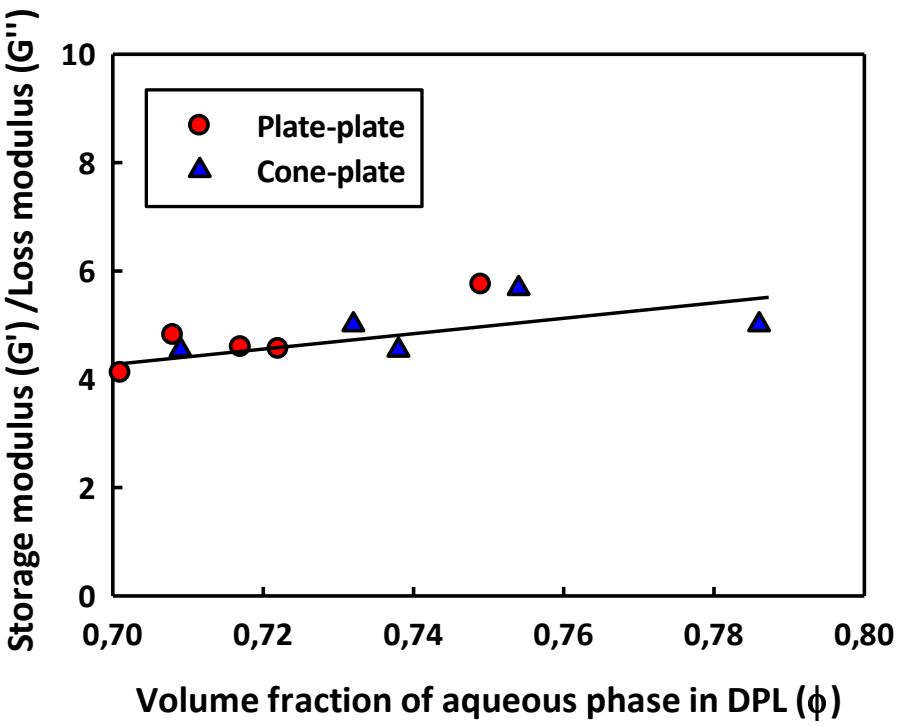

Fig. 12. Average storage modulus ($G^{'}$) and loss modulus ($G^{''}$) ratio over the investigated frequency range from 0.1 Hz to 10 Hz measured by plate-plate and cone-plate geometries for the DPLs contained different aqueous volume fractions (ϕ) (Strain=0.1 %, T=20^{o}C).

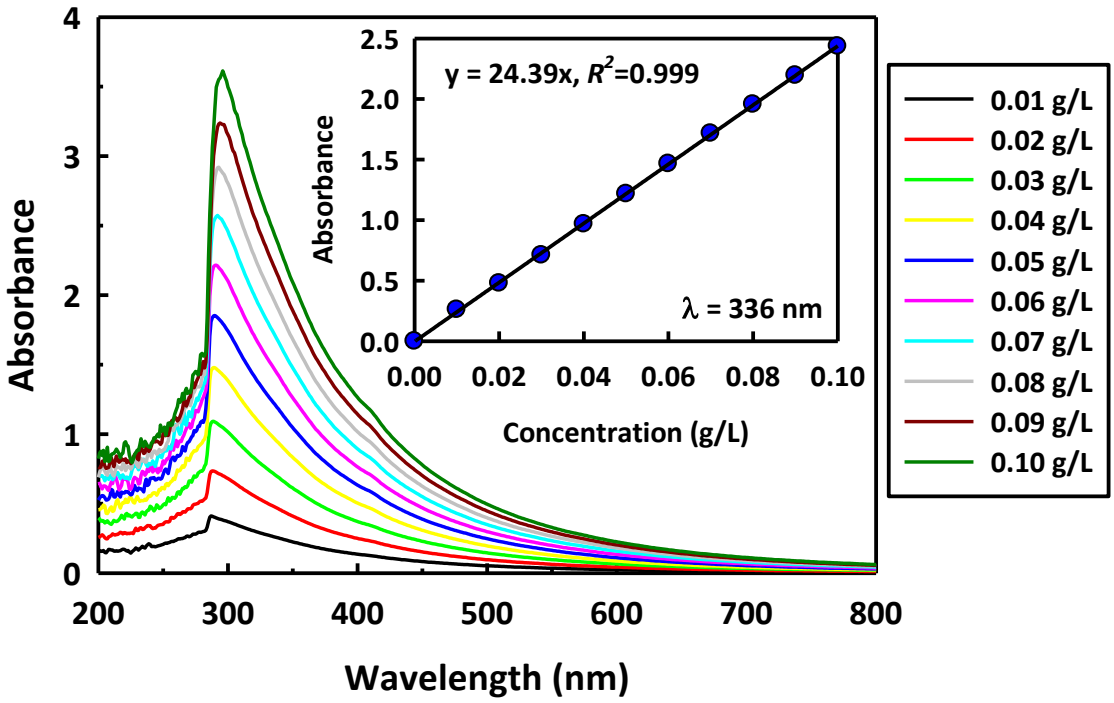

Fig. 13. UV-Vis absorbance spectra of the asphaltene solutions at different concentrations in xylene and the constructed calibration curve at 336 nm (T=20^{o}C).

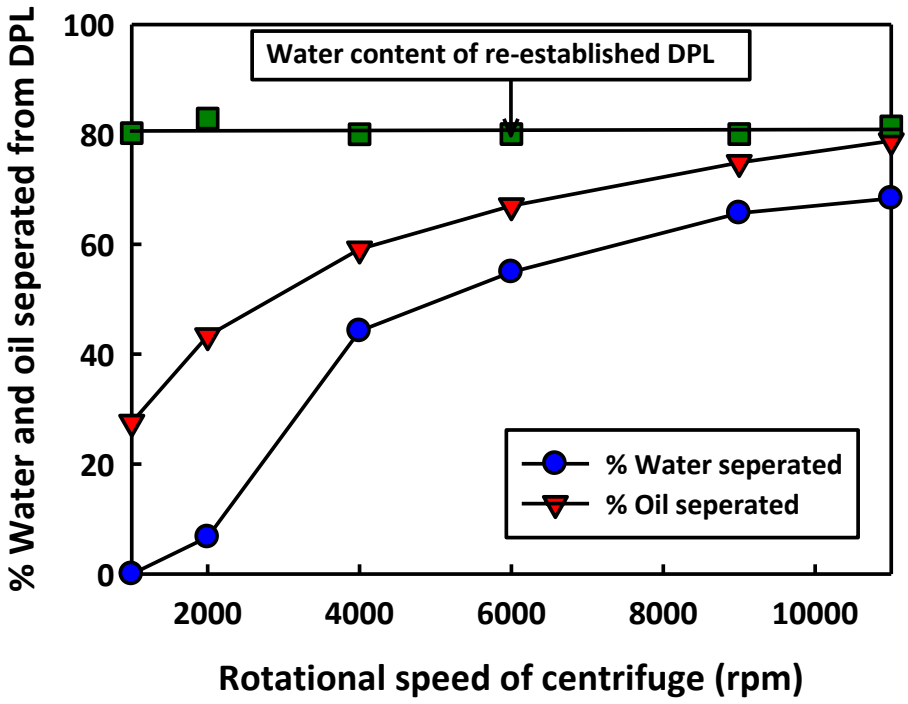

Fig. 14. Separated water and oil percentages from the DPL as a function of rotational speed of centrifuge and water content of the re-established DPL after each centrifugation (Asphaltene concentration in xylene = 8 g/L, Volume of DPL = 10 mL, Aqueous phase volume fraction in the DPL=0.745, T=20^{o}C).

Tables:

Table 1. Physico-chemical properties of the crude oil used to extract the asphaltene in this study.

[a] SARA fractions (wt. %)				[b] Water content (wt. %)	[c] Density
Saturates	Aromatics	Resins	Asphaltenes		
37.4	44.1	16.4	2.5	0.06	0.93

[a] Determined according to the method given by Hannisdal et al. [32]

[b] Determined using the Karl-Fischer titration method.

[c] Determined using the Anton Paar DMA 5000 density meter at 20^{o}C.

Table 2. Elemental composition of the asphaltene used in this study.

Fraction	C	H	N	O	S
% (w/w)	85.3	8.25	1.31	1.87	2.23

Table 3. The yield stress (τ_y), consistency index (K), and flow behaviour index (n) of the DPLs separated from various batch of the asphaltene stabilized emulsions and contained different aqueous phase volume fractions (ϕ) determined from flow curve and oscillatory shear measurements using "plate-plate geometry" (T= 20^{o}C).

ϕ	Flow curves (shear stress vs. shear rate measurements)						Oscillatory shear measurements
	τ_y (Pa)		K (Pa.s)		n		τ_y (Pa)
	Increasing curve	Decreasing curve	Increasing curve	Decreasing curve	Increasing curve	Decreasing curve	
0.701	0.14	0.11	0.14	0.11	0.81	0.83	0.04
0.709	0.15	0.09	0.19	0.14	0.79	0.84	0.06
0.717	0.22	0.18	0.20	0.15	0.79	0.86	0.08
0.722	0.29	0.14	0.21	0.18	0.82	0.85	0.11
0.749	2.60	0.67	0.72	0.45	0.72	0.88	0.67

Table 4. The yield stress (τ_y), consistency index (K), and flow behaviour index (n) of the DPLs separated from various batch of the asphaltene stabilized emulsions and contained different aqueous phase volume fractions (ϕ) determined from flow curve and oscillatory shear measurements using "cone-plate geometry" (T= 20^{o}C).

ϕ	Flow curves (shear stress vs. shear rate measurements)						Oscillatory shear measurements
	τ_y (Pa)		K (Pa.s)		n		τ_y (Pa)
	Increasing curve	Decreasing curve	Increasing curve	Decreasing curve	Increasing curve	Decreasing curve	
0.709	0.05	0.08	0.18	0.16	0.83	0.87	0.06
0.732	0.34	0.29	0.40	0.27	0.78	0.86	0.20
0.738	0.42	0.25	1.81	0.41	0.54	0.85	0.22
0.754	0.50	0.45	1.22	0.78	0.66	0.76	0.66
0.786	N.D.	0.86	N.D.	5.53	N.D.	0.52	1.45

N.D.: The Herschel-Buckley equation (Eq. 8) does not fit quite well the flow curve data.

Table 5. Initial concentration of the asphaltene in oil phase, final concentration of the asphaltene in oil phase after separation of the DPL from the emulsion, aqueous phase volume fraction of the separated DPL, adsorbed amount of the asphaltene in the DPL ($mg.m^{-2}$) and surface area per molecule of the asphaltene (σ) in the DPL determined for various batches of the asphaltene stabilized emulsions (w/o) ($T=20^{o}C$).

Conc. of asphaltene in oil phase ($g.L^{-1}$)	Conc. of asphaltene in oil phase after separation of DPL ($g.L^{-1}$)	Aqueous phase volume fraction of DPL (ϕ)	Adsorbed amount of asphaltene (Γ) in DPL ($mg.m^{-2}$)	Surface are per molecule of asphaltene (σ) in DPL ($Å^2$)
8	6.55	0.768	1.95	64
	6.38	0.778	1.86	67
	6.36	0.786	1.91	65
	6.53	0.791	1.79	69
	6.39	0.808	1.94	64